Alma Mater Studiorum Università di Bologna
Archivio istituzionale della ricerca

Evaluation of 2-(salicylideneimino) thiophenol and other Schiff bases as bronze corrosion inhibitors by electrochemical techniques and surface analysis

12 September 2024

Evaluation of 2-(salicylideneimino) thiophenol and other Schiff bases as bronze corrosion inhibitors by electrochemical techniques and surface analysis

C. Monticelli[a]*, A. Balbo[a], J. Esvan[b], C. Chiavari[c], C. Martini[d], F. Zanotto[a], L. Marvelli[e], L. Robbiola[f]

[a] Centro di Studi sulla Corrosione e Metallurgia "A. Daccò", Università di Ferrara, Via G. Saragat 4/a, 44122 Ferrara, Italia

[b] Centre Interuniversitaire de Recherche et d'Ingénierie des Matériaux, Université de Toulouse, 4 allée Emile Monso, 31030 Toulouse, France

[c] Dipartimento di Beni Culturali, Università di Bologna, via degli Ariani 1, 48121 Ravenna, Italia

[d] Dipartimento di Ingegneria Industriale, Università di Bologna, viale Risorgimento 4, 40136 Bologna, Italia

[e] Dipartimento di Scienze Chimiche e Farmaceutiche, Università di Ferrara, Via L. Borsari 46, 44121 Ferrara, Italia

[f] TRACES lab (CNRS UMR 5608), Université de Toulouse, allées Antonio-Machado, 31058 Toulouse, France.

Keywords

Bronze, corrosion inhibitor, Schiff bases, EIS, XPS.

* Corresponding author

E-mail addresses:

mtc@unife.it (C. Monticelli),

andrea.balbo@unife.it (A. Balbo),

jerome.esvan@ensiacet.fr (J. Esvan),

cristina.chiavari@unibo.it (C. Chiavari),

carla.martini@unibo.it (C. Martini),

zntfrc@unife.it (F. Zanotto)

lorenza.marvelli@unife.it (L. Marvelli)

robbiola@univ-tlse2.fr (L. Robbiola)

Abstract

In this research, different Schiff bases were synthesized and tested as bronze corrosion inhibitors in concentrated synthetic acid rain at pH 3.3. Some of them showed good inhibiting effects, as detected by EIS and polarization curve recording. The most efficient inhibitor (2-(salicylideneimino) thiophenol, SITP) was also tested with addition of sodium dihydrogen phosphate (P). P improved the surface film resistance against breakdown phenomena. XPS and SEM investigations showed that SITP and SITP+P significantly hinder decuprification. Moreover, SITP forms a protective layer on bronze, composed of both Cu(I)-SITP complexes and adsorbed inhibitor molecules. Cu(II) phosphates were also detected with P addition.

1. Introduction

Ancient and modern bronze artefacts are an important part of our cultural heritage and the development of effective protective treatments with no adverse effect on health and environment is still an unresolved issue. This research deals with the identification of new bronze corrosion inhibitors in concentrated synthetic acid rain and represents a first step in a more complex research activity, aiming at developing new non-hazardous protective coatings for outdoor bronze artefacts, entrapping corrosion inhibitors. In a subsequent step of this research, the most efficient substance will be encapsulated in the coatings with the aim to increase their long term protectiveness. Some preliminary results were presented in [1].

Up to now, the most efficient organic inhibitors of bronze corrosion have mainly been azoles and particularly triazoles [2-4], tetrazoles [2, 5], imidazoles [6] and thiadiazoles [2, 5, 7, 8]. The inhibition mechanism of these substances has been investigated above all on copper, as it is the main alloying element in bronze. Chemisorption was found to occur through the electron lone pairs in N atoms and/or through delocalized π-electrons in aromatic rings favoured by the concomitant presence of other heteroatoms with donor nature, like S, either in the ring or in functional groups [9]. In acid solutions, azole adsorption is weak suggesting that it mainly occurs through the deprotonated molecular forms [10-12], except for molecules of very basic nature like imidazoles, which also adsorb significantly in the neutral form [13-15]. Whether azoles adsorb directly on copper metal [16-18] or on a surface cuprous oxide film is still under debate [9,19,20]. Some authors couple the two theories and maintain that, after an initial step of direct adsorption on the metal surface, slow copper oxidation to Cu(I) proceeds and determines the subsequent growth of a polymeric Cu(I)-inhibitor film [21-23], which most likely lies [24-26] on a thin Cu_2O

inner layer. A 24 Å thick Cu(I)-BTA layer doped with Cu_2O was found to grow on copper in neutral chloride solution after short immersion times [27].

In the field of bronze heritage conservation [2,4], BTA and triazole derivatives are the most commonly used inhibitors, even if toxicity concerns have been raised regarding BTA as a result of its leaching into the environment [28] and suspected carcinogenicity to humans [29].

Some substances, belonging to the class of Schiff bases and considered non-toxic to the environment [30], have been proven to be efficient inhibitors of copper corrosion in acidic and neutral solutions of chlorides [19, 30-33]. They are claimed to produce thin protective layers on the metal surface, by forming N–Cu coordinate bonds or π-electron interactions with the surface Cu_2O film [30]. The introduction of a thiol group into the molecular structure favours the inhibitor chemisorption on pure copper from hydroalcoholic solutions [31].

In our laboratory, some Schiff bases were purposely synthesized and investigated as corrosion inhibitors of bronze during 480 h of immersion in concentrated synthetic acid rain. Since some phosphonates mixed with amine substances revealed a synergistic inhibition effect against steel corrosion [34], the onset of a similar synergistic inhibition effect was attempted by adding phosphate ions to the most efficient Schiff base (i.e. 2-salicylideneimine thiophenol, SITP). The composition and microstructure of the bronze substrate used during the tests were comparable to those of Renaissance bronze [5]. When in contact with a concentrated synthetic acid rain, a patina which is very similar to those actually found on ancient bronze artworks develops [35].

The mechanism of SITP corrosion inhibition, in the absence and presence of phosphate ions, was studied not only by electrochemical techniques, but also by scanning electron microscope associated with energy dispersive spectroscopy (SEM-EDS), Raman spectroscopy and X-ray

photoelectron spectroscopy (XPS). These techniques led to a better understanding of the influence of the inhibitor addition against bronze decuprification.

2. Experimental part

2.1 Specimens and aggressive environment

The specimens were cut from an as-cast bronze alloy sheet with composition (91.9 Cu, 2.4 Sn, 1.0 Pb, Zn 2.9, 0.8 Sb, wt.%) and microstructure reproducing those of Renaissance bronze artefacts with cored dendrites of Cu-solid solution with Sn- and Sb- local enrichment, also including Pb globules in the interdendritic spaces, as reported in previous papers [5, 35, 36].

Bronze electrodes were soldered to sheathed copper wires to ensure electrical connection for electrochemical tests and then embedded in epoxy, with an exposed surface area of 1 cm^2. Before immersion in the aggressive solutions, the electrode surface was prepared by grinding with emery papers up to P 1000 grade and then polished with 1 μm diamond powder to a mirror finishing. Finally, they were degreased with ethyl alcohol and washed with deionized water.

The test solution consisted of a tenfold concentrated synthetic acid rain (pH 3.3) indicated as ARX10 and prepared according to the recipe reported in [37]. In ARX10, the ion concentrations were: SO_4^{2-} 19.0 mg L^{-1}, Cl^- 12.7 mg L^{-1}, NO_3^- 46.2 mg L^{-1}, CH_3COO^- 2.3 mg L^{-1}, $HCOO^-$ 0.5 mg L^{-1}, NH_4^+ 10.5 mg L^{-1}, Ca^{2+} 3.4 mg L^{-1}, Na^+ 5.3 mg L^{-1}. The solution temperature was 30 °C.

The Schiff bases tested as corrosion inhibitors were 2-(salicylideneimino) thiophenol (SITP), 2-salicylideneimino) aminophenol (SIAP), 2 - (3-methoxy-salicylideneimino) thiophenol (MSITP), N,N'-O-phenylen-bis(3-methoxy-salicylideneimine) (PMSI) and [2-(2-thiophenyl)imino]-1,2-diphenylethanone (TPIE), with structural formulas reported in **Figure 1**. They were synthesised starting from the corresponding amines and aldehydes in the Inorganic Chemistry Laboratory of

the University of Ferrara and their purity was checked by elemental analysis, Fourier Transform

Infrared (FTIR) spectroscopy and Proton Nuclear Magnetic Resonance (^{1}H NMR) technique. Given

the low Schiff bases solubility, they were always tested as ARX10 solutions saturated at 30 °C and

filtered. The saturation concentrations in ARX10 at 30 °C were 0.7 mM (in the case of SITP), 0.3

mM (SIAP, MSITP, PMSI) and 0.4 mM (TPIE).

The inhibiting efficiency of the most concentrated and most effective substance (SITP) was also

evaluated in the presence of phosphate ions, added as sodium dihydrogen phosphate (NaH$_2$PO$_4$,

henceforward indicated by the label P), at the concentration of 10^{-2} M. The addition of P

determined a negligible increase in solution pH compared to that of the ARX10 solution containing

or not containing the Schiff bases (from 3.3 to 3.6). Reference tests were also carried out in ARX10

in the presence of only 10^{-2} M P.

< **Figure 1**>

2.2 Electrochemical tests

Electrochemical tests were carried out in a conventional thermostated three-electrode cell using a

EG&G potentiostat/galvanostat model 273A, piloted by PowerSuite software. The reference and

auxiliary electrodes were a saturated calomel electrode (SCE) and a Pt sheet, respectively. All the

potential values quoted in the text refer to SCE. Three experiments were carried out under each

experimental condition.

Electrochemical Impedance Spectroscopy (EIS) tests were performed at the open circuit potential

during 480 h exposures to uninhibited and inhibited solutions by applying a voltage perturbation

amplitude of 10 mV (rms) in the frequency range $10^4 – 10^{-3}$ Hz with 5 points per frequency decade.

The spectra were fitted by SAI ZView v.3.5c software, according to the most suitable equivalent circuit, as described in the text.

Ohmic drop-compensated polarization curves were recorded after both 1h immersion and at the end of the 20 days of immersion in uninhibited or inhibited ARX10, always starting from the corrosion potential (E_{cor}) and reaching a cathodic polarization of - 0.300 V vs E_{cor}, in the case of the cathodic branch, and up to a current density of about 3 mA cm^{-2} (or + 0.5 V_{SCE}, the first of the two limits), in the case of the anodic branch. The potential scan rate was 0.167 mV s^{-1}. The Levenburg–Marquardt (LEV) method was applied (by software SAI CView v.3.5c) to properly fit the coupled anodic and cathodic polarization curves to the following equation:

$$j = j_{cor} \left(10^{\frac{E_{cor}-E}{b_a}} - 10^{\frac{E_{cor}-E}{b_c}}\right) \qquad (1)$$

in order to evaluate the corrosion current density, j_{cor} and the anodic and cathodic Tafel slopes (b_a and b_c) [38].

2.3 Surface analyses

A Scanning Electron Microscope (SEM) model ZEISS EVO MA 15, coupled to an Energy Dispersive X-Ray Spectroscopy (EDS) system (Aztec Oxford apparatus, SDD detector, WD 10 mm, EHT 20 kV), was used to characterise non-polarized samples exposed for 480 h to the aggressive solutions with and without inhibitors. Elemental EDS analyses were performed on large surface areas (1.0 × 0.5 mm^2) in order to determine the Cu/Sn wt% ratio before and after exposure to assess the extent of decuprification in each condition.

In addition to this elemental surface investigation, Raman and XPS spectroscopies were also performed to characterize the sample surfaces.

The Raman spectrometer used was a Renishaw InVia connected to a Renishaw SCA (Structural and Chemical Analyzer). The spectra were collected with an Ar$^+$ laser (λ = 514.5 nm) and power output less than or equal to 5 mW, to avoid surface degradation.

XPS analyses were carried out on the first atomic layers of the exposed surfaces, using a monochromatized Al-Kα source (hv= 1486.6 eV) on a ThermoScientific K-Alpha system. The X-ray spot size was about 400 µm in diameter. The photoelectron emission spectra were recorded in direct N(Ec). The pass energy was fixed at 130 eV with a step of 1 eV for surveys, and 40 eV with a step of 0.1 eV for core levels. Ionic sputtering of the surfaces was made with Ar$^+$ ion beam accelerated under 200 eV low current for 30 s, in order to remove carbon surface contamination. XPS data were fitted by using Thermo Scientific^{TM} Avantage Software and Shirley method was used for the background subtraction of all the peaks. Prior to testing, the samples were stored under N_2 to avoid any surface alteration.

3. Results

3.1 Polarization curves

The polarization curves recorded after 1h immersion in uninhibited and inhibited solutions are reported in **Figure 2a** and **b.** In uninhibited ARX10 (blank solution), bronze exhibited a low corrosion current density (j_{cor} of the order of 1 µA cm^{-2}) and a relatively high anodic slope up to about 0.01 V, suggesting the presence of a rather continuous and protective oxide film which is most likely to be a residual of the air-formed one. At 0.01 V, an abrupt anodic slope change occurred denoting the breakdown of the passive film, followed by fast bronze dissolution. The cathodic reaction sustaining bronze corrosion was oxygen reduction, which was under activation

control at the corrosion potential, E_{cor}, and reached a limiting reduction current after about 200 mV of cathodic polarization. This indicated that the surface film on bronze sustained a relatively slow charge transfer process controlling oxygen reduction reaction.

Figure 2a shows that the addition of SITP, MSITP and TPIE determined a significant inhibiting effect on the cathodic reaction, shifting E_{cor} values towards negative values. These Schiff bases also widened the passive potential range, but MSITP and TPIE did not increase the potential of film breakdown (about 0.01 V) while SITP ennobled it to 0.10 V, determining a passive potential range of about 400 mV. On the contrary, PMSI (**Figure 2b**) did not significantly modify the corrosion process in comparison to that observed in the blank solution, and slightly reduced the width of the passive potential range. Finally, the addition of SIAP (**Figure 2b**) stimulated the cathodic process and accelerated the corrosion of bronze due to the shift of E_{cor} up to the potential of film breakdown. Consequently, the test in this last solution was not prolonged over 24 h.

< **Figure 2** >

< **Table 1** >

< **Figure 3** >

The polarization curves recorded after 480 h immersion in the absence and in the presence of the Schiff bases except for SIAP are shown in **Figure 3a**, while **Table 1** reports the electrochemical parameters derived from these curves. In particular, the **Table** collects the E_{cor} and j_{cor} values, the anodic and cathodic Tafel slopes, b_a and b_c, and the inhibiting efficiency values (η), evaluated by the following formula:

$$\eta = \frac{j_{cor,u} - j_{cor,i}}{j_{cor,u}} \times 100 \qquad (2)$$

where $j_{cor,u}$ and $j_{cor,i}$ refer to the corrosion current density evaluated in uninhibited and inhibited solutions, respectively, by applying the Levenburg–Marquardt (LEV) method and equation (1). As an example, in the case of ARX10 in the absence and in the presence of SITP **Figure 3b** shows the comparison between the experimental and calculated polarization curves obtained by fitting. Some limited discrepancies were detected due to noise introduced by ohmic drop compensation, especially around E_{cor}. However, the overall agreement achieved may be considered quite acceptable considering the scope of this research.

Figure 3a shows that in the absence of additives, the anodic and cathodic currents were higher than those recorded at short immersion times (**Figure 2**). The cathodic reaction of oxygen reduction was under mass transport control at E_{cor} as indicated by the very high $|b_c|$ value (**Table 1**) and reached a limit current density of about 10 µA cm^{-2}, after about 100 mV of cathodic polarization. The shape of the anodic curve suggests that bronze was covered by a surface layer of corrosion products (patina), which partially protected the alloy up to about 0.170 V, where a slope change suggested a faster dissolution process. Average j_{cor} values of about 8.3 µA cm^{-2} could be obtained by application of the non linear fitting method (**Table 1**).

After 480 h the different Schiff bases showed variable inhibiting effects towards bronze corrosion, as indicated by the range of j_{cor} and η values reported in **Table 1**. In general, in spite of their low concentrations three of them (SITP, TPIE and MSITP) exhibited significant η values of 99.91, 94.6 and 77.3 %, respectively. The most efficient substance, SITP, clearly behaved as a mixed corrosion inhibitor because it afforded a strong inhibition of both the cathodic and the anodic process, with passive conditions maintained up to a breakdown potential of about + 0.23 V, that is about 60 mV higher than that recorded in uninhibited solution. TPIE and MSITP could also hinder both the

cathodic process, particularly in the case of TPIE, but also the anodic reaction, with the formation of rather protective surface patinas. In both cases, the anodic curves showed a film breakdown potential close to that recorded in SITP solution. Finally, PMSI negligibly inhibited the reaction of oxygen reduction and the anodic polarization curve exhibited a slope of 64.1 mV decade^{-1}, much lower than that recorded in the blank solution.

Since phosphonates and N-containing inhibiting mixtures showed synergistic inhibition of steel corrosion in chloride solution [34], an attempt was made to assess whether a mixture of saturated SITP and 10^{-2} M P would also afford a similar synergistic effect for bronze. For this reason, bronze samples were exposed for 480 h to ARX10 in the presence of either the SITP+P mixture or only P salt. Final polarization curves are collected in **Figure 4**, while the electrochemical parameters derived from these polarization curves are collected in **Table 1.** They show that P alone negligibly inhibited the cathodic reaction in the vicinity of E_{cor}, but under anodic polarization the alloy reached a passivation potential at about + 0.07 V, above which a quite steep anodic slope was obtained with currents slowly increasing from 15 to 100 µA cm^{-2} without the onset of pitting attack up to + 0.5 V. The SITP+ P mixture was very effective, but did not afford any synergistic inhibition because j_{cor} was slightly higher than that obtained with SITP alone (**Table 1**). However, the mixture induced a stable passive condition on bronze which remained unaltered up to potentials nobler than +0.5 V.

< **Figure 4** >

3.2 EIS tests

A nondestructive EIS technique was used to investigate the time evolution of the corrosion process on bronze and to characterize the bronze / aggressive solution interface in ARX10, in the absence and in the presence of the various Schiff bases. In the case of SITP, the influence of P addition was also studied.

As shown in **Figures 5a** and **b**, the dielectric behavior of bronze exposed to uninhibited ARX10 for periods longer than 1h was characterized by three time constants, in accordance with results obtained by other authors in similar environments [6,39,40]. In fact, three loops were detected in the Nyquist plots, in the frequency ranges: $10 - 10^3$ Hz (high-frequency (HF) loop), $10^{-1} - 10$ Hz (medium-frequency (MF) loop), and at frequencies lower than 10^{-1} Hz (low-frequency (LF) arc). The spectra were correctly fitted by the equivalent circuit (EC) reported in **Figure 6a**, where three nested R-CPE (Resistance-Constant Phase Element) couples were present. As the loops in the spectra were depressed semicircles, CPE elements were used instead of capacitances to compensate for surface roughness, porosities and other surface inhomogeneities. The impedance expression of CPE was $Z = [Y(jw)^n]^{-1}$, where $w = 2\pi f$ is the angular frequency, $j = \sqrt{(-1)}$ is the imaginary unit, Y is a frequency independent value and n is a fit parameter with values $0 \leq n \leq 1$, which measure the element deviation from the ideal capacitive behaviour (exhibiting n = 1) [41-43]. For each R-CPE couple, the general equation $C = (R^{1-n} Y)^{1/n}$ was used to convert the Y parameters of the CPE elements into the associated capacitances (with R being the corresponding couple resistance) [40,44].

< **Figure 5** >

< **Figure 6** >

Previous studies allow a physical interpretation of the elements in **Figure 6a** [6,39,40,45,46]. In particular:

- R_s is the solution resistance between the bronze electrode and the reference electrode;

- the R_f - CPE_f couple describes the dielectric properties of a surface corrosion product film (HF time constant), with R_f and C_f corresponding to the resistance and pseudocapacitance values of the surface film;

- the R_t - CPE_{dl} couple is correlated to the charge transfer reaction occurring on bronze (MF time constant) and R_t and C_{dl} are the charge transfer resistance and the capacitance of the double layer at the metal-electrolyte interface;

- the R_F-CPE_F pair (LF time constant) refers to the faradaic reactions of oxidation – reduction involving the surface corrosion products (likely related to the redox reaction between Cu and Cu(I) ions, the latter incorporated into the surface film based on cuprite, Cu_2O, in the blank solution); therefore R_F and C_F are the resistance of the faradaic reactions and the related pseudocapacitance value, respectively.

The n exponent values in CPE analytical expressions used to fit the depressed features of experimental Nyquist plots fall within the range 0.54 – 1, in analogy to previous results achieved on bronze in uninhibited and inhibited synthetic acid rain [6,39,47].

The evolution of the bronze corrosion behavior in uninhibited ARX10 can be interpreted by discussing the EIS fitting results, also in the light of the trends shown by the polarization curves (**Figures 2** and **3**).

First af all, **Figure 5a** shows a time evolution of the solution resistance values (R_s, corresponding to the high frequency intercept of the spectra with the real axis). In fact, from 1 to 48 h of immersion,

R_s passed from 500 to about 800 ohm cm^2, due to a concomitant solution pH increase from 3.3 to about 5.3, induced by the oxygen reduction reaction sustaining corrosion. At even longer immersion times (**Figure 5b**), R_s values remained more or less constant because of the buffering effect of dissolved copper cations determining a pH stabilization.

After 1h immersion in ARX10, only the MF and LF time constants were distinguished in the EIS spectrum (**Figure 5a**, inset), suggesting that the surface film had a negligible effect on the electrode impedance. The R_f - CPE_f couple was, therefore, omitted and the EC adopted is that reported in **Figure 6b.** The results of the best fitting procedure are also included in **Figure 5**. Quite similar results have been obtained by other authors in comparable environments [6,46]. The fitting parameters are reported in **Figure 7**, together with the R_p values calculated as the sum: $R_p = R_f + R_t + R_F$ [40, 46-49]. Although at 1 h immersion a clear time constant related to the surface film was not detected, bronze exhibited a passive behaviour as evidenced by the high anodic slope in the 1 h anodic polarization curve (**Figure 2**). The surface film, likely residual of the air-formed oxide film, determined a relatively high charge transfer resistance (a high R_t at 1h immersion), thus justifying the low cathodic currents in the blank polarization curves of **Figure 2** [37]. At increasing immersion times, the film underwent a fast alteration in contact with the aggressive solution because after 2 h immersion R_t and R_p had already shown a significant decrease.

< **Figure 7** >

Until about 260 h, rather low and constant R_f and R_t values were achieved. They then tended to increase slightly with time as a consequence of the accumulation of corrosion products hindering the alloy oxidation. This was in agreement with the shape of the anodic polarization curve recorded on bronze after 480 h of immersion (**Figure 3**), which exhibited a relatively high anodic

slope of 90.2 mV/decade. The decrease in C_f pseudocapacitance values after 360 h confirmed the increase in film thickness at long immersion times, while the C_{dl} diminution, particularly in the second half of the immersion, was most likely a consequence of the decrease in the surface area of the active anodic regions under the surface film.

R_F, connected to the resistance of the faradaic reaction of interchange between Cu and Cu(I), significantly decreased during most of the immersion period because the Cu_2O film, which is expected to have a high faradaic activity, grew on the surface and caused an increase in region areas where the reaction may occur. A final increase in R_F trend may have been connected to the final decrease in film porosity with a consequent decrease in the electrolyte accessibility to the metal/Cu_2O interface. This variation of the metal/Cu_2O interface area also affected C_F which accordingly showed an opposite trend to R_F, in particular an initial fast, followed by a slow increase and a final decrease.

< **Figure 8** >

In SITP solution, due to the strong inhibition of the corrosion process, a limited pH variation was detected during bronze immersion (final pH values = 3.5) and consequently rather constant R_s values (in the range 450-550 ohm cm^2) were measured. With this very efficient inhibitor only the HF and MF loops were detected, while the LF loop connected to the faradaic reactions was absent at all immersion times. This suggests that the inhibitor adsorption produces a highly stable surface film with low Cu(I) ⇆ Cu reactivity. The evolution of the SITP spectra is shown in **Figure 8a**, which clearly evidences an increase in bronze corrosion resistance during time. The two time constant-EC reported in **Figure 6c** was used for curve fitting and the parameters achieved by data interpolation are reported in **Figure 7**, where they can be compared to those in the blank solution.

The high and increasing corrosion resistance of bronze was connected to a high R_t which rose up to about 5 MΩ cm^2 and to R_f, which increased with time by more than two orders of magnitude and finally reached a value over 1 MΩ cm^2. This suggests that SITP appears to produce a protective surface film which hinders charge transfer from the very beginning of the immersion. The concomitant limited decrease in C_f pseudocapacitance values suggests that the thickness of the SITP film grows only slightly with time and its increasing resistance is likely connected to a progressively more compact and resistive nature. C_{dl} decreased by one order of magnitude with time, which may reasonably be put down to a decrease in surface area on which charge transfer may occur while the film density increases and/or to a progressive substitution of water molecules (with high dielectric constant) by adsorbed organic inhibitor molecules (with low dielectric constant) within the double layer.

Given its interesting anodic behavior, the inhibition mechanism of the mixture SITP+P was also investigated by means of EIS spectra fitting. In this case, during bronze immersion no pH variation and rather constant R_s values were detected. These latter values were lower than those measured in SITP solution (about 200 ohm cm^2), due to the presence of 10^{-2} M P (sodium dihydrogen phosphate salt). Selected spectra among those recorded during the 480 h immersion period are presented in **Figure 8b**. They are quite different from those recorded in the presence of SITP alone, as they are again best fitted by the three time constant-EC of **Figure 6a**. Therefore, although in this solution bronze underwent a much slower corrosion process than in the blank, the electrode impedance was affected by the same contributions found in the blank solution: the dielectric properties of a surface film, a charge transfer process at the electrode surface and a

faradaic reaction involving the surface film. The fitting parameters can be compared to those obtained in the presence of SITP alone and in the blank solution in **Figure 7**.

Within 72 h of immersion, R_f was higher than in SITP solution (values around 40-50 kΩ cm^2) and then set at about 30 kΩ cm^2. These final values were more than one order of magnitude lower than the final ones achieved in SITP solution, while only slightly lower R_t values were obtained, setting at about 1 MΩ cm^2. R_F was always higher than R_t and followed the same R_t trend. The presence of the R_F-C_F couple in the EC suggests that in SITP+P solution the film exhibits a faradaic activity, but is less susceptible to redox processes than in the blank solution, as indicated by much higher R_F and much lower C_F values. Within the initial 2-3 days of exposure, C_f and C_{dl} decreased slowly and then remained more or less constant, suggesting a limited increase in the film thickness and a contemporary decrease in the metal surface area available for charge transfer. All these findings indicate that the addition of P to SITP solution changed the characteristics of the surface film. In particular, even at short immersion times P contributed to producing a resistive film which did not then evolve significantly. Although this film maintained a low faradaic activity it was higher than that of the SITP film. In general, these variations induced high R_p values (**Figure 7d**), even higher than those presented by SITP alone within 3 days of immersion, but, in accordance with polarization curve results, they were comparable to those obtained by SITP during long immersion times.

With the exception of SITP, the other Schiff bases showed EIS spectra with three time constants, like those in the blank solution, and could be fitted with the EC in **Figure 6a.** As an example, **Figure 9** shows the agreement between the experimental spectra obtained in the presence of the Schiff

bases at the end of the immersion period and those obtained by the fitting procedures (χ^2 values

≤ 0.0007).

$<$ **Figure 9** $>$

$<$ **Figure 10** $>$

The R_p (calculated as the sum of R_f, R_t and R_F) and the corresponding E_{cor} values obtained on

bronze with time in the absence and presence of all Schiff bases are reported in **Figure 10**.

In comparison to the blank, SIAP addition did not modify bronze corrosion behavior in ARX10 (as

also indicated by the spectrum in the inset of **Figure 9**); this was likely due to its low concentration

and scarce adsorption capability. Instead, TPIE and MSITP, but also PMSI to a limited extent,

presented an inhibition effect, in agreement with the results of the polarization curves. The

concurrent E_{cor} evolution exhibited quite negative initial values, often more active than those in the

blank, suggesting that they initially acted as cathodic inhibitors. Their surface films then became

more protective and their E_{cor} values reached and exceeded those in the blank solution. In

conclusion, as also indicated by the recorded polarization curves, SITP, TPIE and MSITP act as mixed

corrosion inhibitors.

The inhibiting efficiencies of the Schiff bases and SITP+P formulation after 480 h immersion

calculated from R_p values ($R_{p,i}$ in inhibited and $R_{p,u}$ in uninhibited blank solutions) by the formula:

$$\eta_{R_p} = \frac{R_{p,i} - R_{p,u}}{R_{p,i}} \times 100 \qquad\qquad (3)$$

are given in **Table 1**. They are in overall good agreement with those achieved from polarization

curve analysis and confirm them.

3.3 SEM-EDS analysis

Figure 11 collects SEM observations obtained on unexposed bronze samples and on samples after 1h or 480 h of immersion in ARX10 solution, both in the absence of inhibitors and in the presence of SITP or SITP + P. **Figure 11 a**, related to unexposed bronze, clearly shows that the alloy was an α-cored bronze with dendritic microstructure, with Sn- an Sb- local enrichment also revealing the Pb globules (white spots in the BSE image of **Figure 11 a**) in the interdendritic regions.

 In ARX10 the corrosion of uninhibited bronze (**Figure 11 b** and **c**) was significant and mainly localized in the core of dendritic regions and at Pb globules. The latter attack is more visible at short immersion times (**Figure 11 b**), where many small black holes were visible in the interdendritic region, due to the dissolution of the white Pb globules clearly evident on unexposed bronze (**Figure 11 a**). This behavior is in agreement with the lower nobility of Pb in comparison to Cu, as assessed during tests on pure metals in ARX10 [35]. The corrosion attack was quite limited in SITP solution (**Figure 11 d** and **e)**. In this case, only partial Pb globule dissolution occurred at long immersion times leaving a few small holes in the corresponding areas. In the presence of the SITP + P inhibiting mixture (**Figure 11 f** and **g)**, the corrosion attack was also very light and, at the end of the immersion, was localized on Pb while the visible dendritic aspect vanished.

Overall, the SEM-EDS analysis after 480 h of immersion revealed the presence of chlorides at a concentration of 0.3 ± 0.1 wt.% on the surface of the sample exposed to non-inhibited solution, while in the presence of SITP and SITP + P these aggressive anions were not detectable. Moreover, in the absence of inhibitors, the phenomenon of decuprification took place on the bronze surface with a reduction in the Cu / Sn wt.% ratio from 34.3 (before exposure) to 15.1 (after 480 h of exposure to ARX10). Instead, after 480 h in the presence of inhibitors, this ratio remains equal to

34.3 in the presence of SITP, and was slightly reduced to 29.4 in the presence of SITP + P. This confirms the lower dissolution of copper from the alloy in the presence of SITP or SITP+P compared to the blank solution.

< **Figure 11** >

3.4 Raman spectroscopy

Raman spectroscopy performed on bronze exposed for 480 h in ARX10 confirmed the presence of typical products found in outdoor bronze patinas. Large crystals of Cu_2O and few isolated crystals of posnjakite ($Cu_4(SO_4)(OH)_6\cdot(H_2O)$)) were found in the core of dendrites, while Cu_2O and traces of nanocrystalline $SnO_x\cdot(H_2O)_y$ were detected in the interdendritic regions.

Raman spectra on SITP-protected bronze showed very pronounced fluorescence bands, suggesting the presence of a surface film containing the organic inhibitor. Also in the case of SITP+P, the Raman spectra were poorly readable, due to the presence of intense fluorescence bands.

3.5 XPS spectroscopy

In order to obtain information on the inhibition mechanism occurring on bronze, the XPS technique was applied on unexposed samples and on samples exposed for 480 h to ARX10, both in the absence and in the presence of SITP or SITP + P.

< **Figure 12** >

As regards the unexposed bronze, the surface XPS analysis (survey in **Figure 12 a**) detected the presence of Cu, Pb and Sn among the alloying elements, and C and O as environmental contaminants. The presence of Zn or Sb was not highlighted. By analyzing the areas of the

deconvoluted profiles in the high-resolution spectra (core levels, in **Figure 13**), it was possible to quantify each peak component in atomic percentages, as summarized in **Table 2**, together with the corresponding binding energies (BE) [36]. Cu and Sn were detected on the surface both in the metallic and oxidized state (**Table 2**) while Pb was mainly present as an oxide, suggesting that surface polishing and air oxidation produces a thin film of corrosion products. Cu 2p core level and Auger spectra (Cu LMM) are reported in **Figures 13 e** and **f**, respectively. The former spectrum showed a high peak at 932.5 eV and no shake-up satellite peak at 940-944 eV, suggesting the possible presence of Cu(I) and/or Cu(0) [50,51]. The Auger Cu $L_3M_{4,5}M_{4,5}$ signals at 916.8 eV and 918.7 eV (Kinetic Energy, KE) well corresponded to a mix of Cu(I) and Cu(0) species, respectively [50,52]. **Figure 13 g** shows quite small Sn3d signals (Sn3d$_{5/2}$ at 486 eV and Sn3d$_{3/2}$ at 494 eV). The deconvolution of Sn 3d$_{5/2}$ (**Figure 13 g**) suggested the concomitant presence of Sn(0) at 484,7eV and Sn(II) at 485,8 eV, both in negligible amounts (**Table 2**) [53-57]. Instead, the core level spectrum of Pb 4f (**Figure 13 h**) showed a peak at 138.1 eV (Pb4f$_{7/2}$) to be ascribed to oxidized Pb and revealed that no metallic Pb was present on the surface [58,59]. This film constituted of limited Cu(I), Sn(II) and Pb oxide species was most likely still present on bronze after 1h immersion in ARX10 and was responsible for the significant bronze corrosion resistance shown by the polarization curves.

＜ **Figure 13** ＞

＜ **Table 2** ＞

A quite different film was present after long immersion periods in the blank solution (survey spectrum in **Figure 12 b**). In fact, beside surface C contamination (core level spectrum in **Figure 13 a**), this film was characterized by the presence of a small N 1s peak at 399.6 eV, compatible with

the deposition of small amounts of ammonium compounds after reaction with ammonium ions in ARX10 (**Figure 13 b**), and a high O1s peak at 531.0 eV (**Figure 13 c**), compatible with oxide formation [36]. Cu 2p core level spectrum (**Figures 13 e**) showed a high peak at 932.3 eV and a smaller one at 934.5 eV, with a significant shake-up satellite peak at 940-944 eV, suggesting the concomitant presence of Cu(I)/Cu(0) and Cu (II) species. The Auger Cu $L_3M_{4,5}M_{4,5}$ signal at 916.8 eV (kinetic energy, KE) and the shoulder at lower KE suggested the presence of Cu(I) and Cu(II) compounds [60]. Core level spectra of Sn 3d (**Figure 13 g**), Pb 4f (**Figure 13 h**) and Sb 3d (the last one not reported in **Figure 13**) showed peaks at 486.7 eV ($Sn3d_{5/2}$), 138.5 eV ($Pb4f_{7/2}$) and 540.1 eV ($Sb3d_{3/2}$), respectively, indicating the presence of Sn(IV) [53-57], Sb(III) [61] and Pb) [58,59] oxides. As regards Pb, the binding energies of Pb oxides were too close to each other to allow for a precise attribution, but, on the basis of the E_{cor} values of bronze in ARX10, the presence of Pb(II) (PbO-like) species was more likely [62].

The XPS results reported in **Table 2** confirm the surface decuprification of bronze due to corrosion revealed from the SEM-EDS analysis. The Cu/Sn atomic ratio decreased from about 29 in the unexposed sample to 1.16 after exposure to the blank solution. Also Pb underwent a preferential dissolution because of a concurrent significant decrease in Pb/Sn ratio.

After 480 h of immersion in SITP solution (survey in **Figure 12 b**), XPS spectra revealed the formation of a SITP-containing film, as indicated by the increase in the content of the inhibitor elements. In fact, an increase in the N 1s peak at 399.2 eV, related to organic N-C bonds [18,27,50] (**Figure 13 b**), and a rise in specific C 1s and S 2p signals were detected. In particular (**Figure 13 a**), instead of the C1s peak at 287.5 eV related to surface contaminants which almost disappeared, high C 1s peaks at 284.4 eV and 286.0 eV were obtained: the former corresponding to organic C-C

and C-H bonds, and the latter related to C-O, C-S and C-N bonds [52]. The intense S $2p_{3/2}$ peak at 163.5 eV was also related to S-C and S-H bonds of the inhibitor, while the shoulder at 162.3 eV suggested the interesting formation of coordination bonds of S-Cu type [50,52]. The third shift of S 2p transition was indicative of the deposit of quite limited amounts of sulphates as corrosion products (**Figure 13 d**) [63]. Analysis of the Cu 2p core level (**Figures 13 e**) disclosed a small peak (much smaller than in the blank) at 932.7 eV and a shoulder at 934.5 eV, with a tiny shake-up satellite peak at 940-944 eV. This spectrum, in association with the Auger Cu $L_3M_{4,5}M_{4,5}$ signal at 916.0 eV (KE) (**Figure 13 f**), was indicative of the predominant presence of Cu(I) species over Cu (II) species (**Table 2**) [60], meaning, therefore, that the surface film was essentially composed of Cu(I)-SITP complexes based on Cu(I)-S bond formation. The intense S $2p_{3/2}$ at 163.5 eV, correlated to S-H and/or S-C, was even more pronounced than that related to the S-Cu(I) structure, suggesting the concomitant presence of adsorbed SITP molecules in the film not involved in complex formation. This would also justify the high N / Cu(I) ratio (much higher than 1) again correlated to the presence of adsorbed SITP molecules, in addition to Cu(I)-SITP complexes. The XPS analysis also detected small amounts of sulphates, most likely Cu(II) salts.

In the presence of SITP + P, quite similar results were achieved, confirming the formation of a SITP film of adsorbed molecules and Cu(I)-complexes. However, in this case the atomic percentages of N atoms and S atoms related to the inhibitor (i.e. both S-Metal and S-H/S-C bonds) and particularly the Cu(I) species (likely involved in the complex formation) were lower than in the sample exposed to SITP. This would suggest that both the overall SITP amount and particularly the relative quantity of Cu(I)-SITP complexes per adsorbed molecules were smaller than in the case of the SITP alone. Thus, a thinner SITP film is to be expected with a smaller Cu complex fraction. Again, in

comparison to SITP sample, the SITP+P sample also showed slightly higher amounts of Cu(II) ions and S atoms involved in sulphate species. Finally, a limited but significant atomic percentage of phosphorus atoms ascribed to phosphates [64] in the film was detected, most likely connected to the surface precipitation of Cu(II) phosphates at film defects where the concentration of dissolved Cu(II) ion was higher. This mechanism of defect healing may have been present in the film since the beginning of the immersion.

In agreement with SEM observation, no Pb signal was detected, in either SITP or SITP+P solutions, due to its significant dissolution after long immersion times, as previously evidenced by SEM observation (**Figure 11**).

4. Discussion

The investigated Schiff bases afford quite different inhibiting efficiency (η) values, as a result of their different concentrations and molecular structures. In spite of their limited solubility determining low saturation concentrations, high η values of 77.3, 94.6 and 99.91 % are obtained by addition of MSITP, TPIE and SITP, respectively, in good agreement with η_{Rp} values, meaning that small amounts of these substances are sufficient to protect bronze.   These substances contain a mercapto group in the molecule, which ensures a stronger chemisorption on bronze, due to its high chemical affinity with Cu cations on bronze surface. In the case of SITP, exhibiting the highest solubility, the best inhibition performances were accordingly achieved. Polarization curves recorded after 480 h immersion in ARX10 show that these three substances act as mixed corrosion inhibitors and increase the potential of surface film breakdown by chlorides on bronze.

By addition of P to SITP solution, excellent η quite close to that in SITP solution and a remarkable increase in breakage potential is achieved. Therefore, the inhibition mechanisms of both SITP and SITP+P additives were investigated by a combination of electrochemical and surface analysis techniques.

Surface analyses show that these substances induce a strong modification of the surface film, which in the blank solution is largely composed of Cu_2O, hydrated SnO_x, PbO-like oxide. According to XPS results, the surface film formed in SITP solution contains both Cu(I)-SITP complexes, based on Cu(I)-S bond formation, and adsorbed SITP molecules. Quite similar results have been obtained by other authors [65] with different S-containing organic inhibitors of copper corrosion, which were reported to produce duplex organic films, including a first chemisorbed layer, on top of which a physisorbed multilayer grows. The stability of the multilayer arises because of π-stack interactions between aromatic rings and Van der Waals bonds between polarizable substitutional functional groups [19, 66]. EIS analysis clearly highlights that in SITP solution the film builds up with time and is quite stable, with negligible Cu(I) $\leftrightarrows$ Cu reactivity. Despite the slow growth, it is able to hinder charge transfer and offers high protectiveness already at short immersion times. The addition of P to SITP solution determines the formation of a thinner surface film (as suggested by XPS results and by the relatively small R_f values obtained by EIS), again composed of a first Cu(I)-SITP complex layer, covered by adsorbed SITP molecules. In comparison to the film in SITP solution, the presence of a smaller fraction of Cu(I)-SITP complex could negatively affect the adhesion of the film on bronze, thus justifying its higher faradaic activity. However, the precipitation of Cu(II) phosphate at flaws of the inhibitor film helps to limit the solution access to the metal surface, so maintaining high R_t and finally high overall R_p values. Pore plugging by Cu(II)

phosphate precipitation is stimulated during anodic polarization, leading to strong passive conditions.

5 Conclusions

1. Among the new Schiff bases specifically synthesized and tested as bronze corrosion inhibitors in tenfold concentrated synthetic acid rain (ARX10), those containing a mercapto group exhibit good inhibiting efficiencies during 480 h immersions. In particular, SITP characterized by the highest solubility (about 0.7 mM, in comparison to 0.4 mM of TPIE and 0.3 mM of MSITP) shows an inhibiting efficiency value of almost 100 %.

2. SITP protects bronze by forming a surface film containing both Cu(I)-SITP complexes and SITP molecules, the latter most likely physisorbed on the first Cu(I)-SITP layer.

3. In the presence of SITP and sodium dihydrogen phosphate (P), bronze results more resistant against localized attack.

4. In SITP+P solution, a SITP thinner film forms on bronze. P determines the precipitation of Cu(II) phosphates at flaws of the surface film, particularly under anodic polarization.

5. SITP and SITP+P addition significantly hinders bronze decuprification.

Acknowledgments

Data avalilability

The raw/processed data required to reproduce these findings cannot be shared at this time as the data also form part of an ongoing study.

6 References

[1] C. Monticelli, V. Grassi, G. Mavilia, F. Zanotto, A. Balbo, Entrapment of corrosion inhibitors in silane coatings to improve bronze corrosion protection, Proc. of EUROCORR 2017 & 20th ICC & Process Safety Congress 2017, 3-7 Sept, 2017, Prague, Paper n. 82386.

[2] S. Golfomitsou, J. F. Merkel, Synergistic effects of corrosion inhibitors for copper and copper alloy archaeological artefacts, Proceedings of Metal 2004, National Museum of Australia Canberra ACT, 4-8 October, 2004, 344-368.

[3] K. Rahmouni, N. Hajaji, M. Keddam, A. Srhiri, H. Takenouti, The inhibiting effect of 3-methyl 1,2,4-triazole 5-thione on corrosion of copper in 3% NaCl in presence of sulphide, Electrochim. Acta 52 (2007) 7519. https://doi.org/10.1016/j.electacta.2006.12.079.

[4] C. Degrigny, V. Argyropoulos, P.Pouli, M. Grech, K. Kreislova, M. Harith, F. Mirambet, N. Haddad, E. Angelini, E. Cano, N. Hajjaji, A. Ciringiroglu, A. Almansour, L. Mahfoud, The methodology of the PROMET project to develop/test new non-toxic corrosion inhibitors and coatings for iron and copper alloy objects housed in Mediterranean museums, Proceedings of Metal 2007, Rijksmuseum, Amsterdam, 2007, p.31.

[5] A. Balbo, C. Chiavari, C. Martini, C. Monticelli, Effectiveness of corrosion inhibitor films for the conservation of bronzes and gilded bronzes, Corros. Sci. 59 (2012) 204. https://doi.org/10.1016/j.corsci.2012.03.003.

[6] K. Marušić, H. Otmačić Curković, H. Takenouti, Inhibiting effect of 4-methyl-1-p-tolylimidazole to the corrosion of bronze patinated in sulphate medium, Electrochim. Acta 56 (2011) 7491. https://doi.org/10.1016/j.electacta.2011.06.107.

[7] L. Ying, F. Haitao, Z. Yifan, W. Wuji, Study on the inhibiting behavior of AMT on bronze in 5% citric acid solution, J Mat. Sci. 38 (2003) 407– 411. https://doi.org/10.1023/A:1021803211415.

[8] D.C.B. Do Lago, L.F. De Senna, E.C.S. Soares, L.F. Da Silva, D.S. Fernandes, A.S. Luna, E. D'elia, The use of experimental design for the study of the corrosion of bronze pretreated with AMT in artificial rainwater, Progr. Org. Coat. 76 (2013) 1289. https://doi.org/10.1016/j.porgcoat.2013.03.032.

[9] M.M. Antonijević, S.M. Milić, M.B. Petrović, Films formed on copper surface in chloride media in the presence of azoles, Corros. Sci. 51 (2009) 1228-1237. https://doi.org/10.1016/j.corsci.2009.03.026.

[10] J.B. Cotton, I.R. Scholes, Benzotriazole and related compounds as corrosion inhibitors for copper, Brit. Corros. J. 2 (1967) 1–5. https://doi.org/10.1179/000705967798327235.

[11] F. Zucchi, G. Trabanelli, M. Fonsati, Tetrazole derivatives as corrosion inhibitors for copper in chloride solutions, Corros. Sci. 38 (1996) 2019-2029. https://doi.org/10.1016/S0010-938X(96)00094-7.

[12] R. Subramanian, V. Lakshminarayanan, Effect of the adsorption of some azoles on copper passivation in alkaline medium, Corros. Sci. 44 (2002) 535-554. https://doi.org/10.1016/S0010-938X(01)00085-3.

[13] N. Kovačević, A. Kokalj, The relation between adsorption bonding and corrosion inhibition of azole molecules on copper, Corros. Sci. 73 (2013) 7–17. https://doi.org/10.1016/j.corsci.2013.03.016.

[14] N. Kovačević, I. Milošev, A. Kokalj, How relevant is the adsorption bonding of imidazoles and triazoles for their corrosion inhibition of copper? Corros. Sci. 124 (2017) 25–34. https://doi.org/10.1016/j.corsci.2017.04.021

[15] M.B. Petrović Mihajlović, M.B. Radovanović, Ž.Z. Tasić, M.M. Antonijević, Imidazole based compounds as copper corrosion inhibitors in seawater, Journal of Molecular Liquids 225 (2017) 127–136. https://doi.org/10.1016/j.molliq.2016.11.038

[16] B.-S. Fang, C.G. Olson, D.W. Lynch, A photoemission study of benzotriazole on clean copper and cuprous oxide, Surface Science 176, (1986) 476-490. https://doi.org/10.1016/0039-6028(86)90050-6

[17] D. Tromans, R.-H. Sun, Anodic Polarization Behavior of Copper in Aqueous Chloride/Benzotriazole Solutions, J. Electrochem. Soc. 138 (1991) 3235-3244. https://doi.org/10.1149/1.2085397

[18] L. Tommesani, G. Brunoro, A. Frignani, C. Monticelli, M. Dal Colle, On the protective action of 1,2,3-benzotriazole derivative films against copper corrosion, Corros. Sci. 39 (1997) 1221-1237. https://doi.org/10.1016/S0010-938X(97)00022-X

[19] M. M. Antonijević, M. B. Petrović, Copper Corrosion Inhibitors. A review, Int. J. Electrochem. Sci., 3 (2008) 1 – 28. http://www.electrochemsci.org/papers/vol3/3010001.pdf

[20] M. Finšgar, I. Milošev, Inhibition of copper corrosion by 1,2,3-benzotriazole: A review, Corros. Sci. 52 (2010) 2737–2749. https://doi.org/10.1016/j.corsci.2010.05.002

[21] G. Xue, J. Ding, P. Lu, J. Dong, SERS, XPS and electroanalytical studies of the chemisorption of benzotriazole on a freshly etched surface and an oxidized surface of copper, J. Phys. Chem. 95 (1991) 7380–7384. https://doi.org/10.1021/j100172a050

[22] Z. Chen, L. Huang, G. Zhang, Y. Qiu, X. Guo, Benzotriazole as a volatile corrosion inhibitor during the early stage of copper corrosion under adsorbed thin electrolyte layers, Corros. Sci. 65 (2012) 214–222. https://doi.org/10.1016/j.corsci.2012.08.019

[23] H.Bi, G.T.Burstein, B.B.Rodriguez, G.Kawaley, Some aspects of the role of inhibitors in the corrosion of copper in tap water as observed by cyclic voltammetry, Corros. Sci. 102 (2016) 510-516. https://doi.org/10.1016/j.corsci.2015.11.005

[24] A.D. Modestov, G.-D. Zhoua, Y.-P. Wua, T. Notoya, D.P. Schweinsberg, A study of the electrochemical formation of Cu(I)-BTA films on copper electrodes and the mechanism of copper corrosion inhibition in aqueous chloride/benzotriazole solutions, Corros. Sci. 36 (1994) 1931-1946. https://doi.org/10.1016/j.corsci.2015.11.005

[25] M. Finšgar, S. Peljhan, A. Kokalj, J. Kovač, I. Milošev, Determination of the Cu_2O thickness on BTAH-inhibited copper by reconstruction of Auger electron spectra, J. Electrochem. Soc. 157 (2010) C295–C301. https://doi.org/10.1149/1.3463718

[26] M. Finšgar, D. Kek Merl, 2-Mercaptobenzoxazole as a copper corrosion inhibitor in chloride

solution: Electrochemistry, 3D-profilometry, and XPS surface analysis, Corros. Sci. 80 (2014) 82–95.

https://doi.org/10.1016/j.corsci.2013.11.022

[27] T. Kosec, D. Kek Merl, I. Milošev, Impedance and XPS study of benzotriazole films formed on

copper, copper–zinc alloys and zinc in chloride solution, Corros. Sci. 50 (2008) 1987–1997.

https://doi.org/10.1016/j.corsci.2008.04.016

[28] D.A. Pillard, J.S. Cornell, D.L. Dufresne, M.T. Hernández, Toxicity of benzotriazole and

benzotriazole derivatives to three aquatic species, Water Res. 35 (2001) 557.

https://doi.org/10.1016/S0043-1354(00)00268-2

[29] Health Council of the Netherlands: 1,2,3-Benzotriazole. Health-based recommended

occupational exposure limit. The Hague: Health Council of the Netherlands, 2000; publication

no.2000/14OSH. ISBN 90-5549-348-1.

[30] H. Ma, S. Chen, L. Niu, S. Zhao, S. Li, D. Li, Inhibition of copper corrosion by several Schiff bases

in aerated halide solutions, J. Appl. Electrochem. 32 (2002) 65-72.

https://doi.org/10.1023/A:1014242112512

[31] C. Monticelli, G. Brunoro, A. Frignani, A. Marchi, The inhibitive action of some Schiff Bases and

amines towards the corrosion of copper in an aqueous alcoholic medium, Surf. Technol. 27, (1986)

175. https://doi.org/10.1016/0257-8972(86)90128-3

[32] Z. Quan, S. Chen, Y. Li, X. Cui, Adsorption behaviour of Schiff base and corrosion protection of

resulting films to copper substrate, Corros. Sci. 44 (2002) 703-715. https://doi.org/10.1016/S0010-

938X(01)00077-4

[33] M. Ehteshamzade, T. Shahrabi, M.G. Hosseini, Inhibition of copper corrosion by self-assembled films of new Schiff bases and their modification with alkanethiols in aqueous medium, Appl. Surf. Sci. 252 (2006) 2949. https://doi.org/10.1016/j.apsusc.2005.05.003

[34] N. Ochoa, F. Moran, N. Pébère, The synergistic effect between phosphonocarboxylic acid salts and fatty amines for the corrosion protection of a carbon steel, J. Appl. Electrochem. 34 (2004) 487. https://doi.org/10.1023/B:JACH.0000021702.49827.11

[35] C. Chiavari, A. Balbo, E. Bernardi, C. Martini, M.C. Bignozzi, M. Abbottoni, C. Monticelli, Protective silane treatment for patinated bronze exposed to simulated natural environments, Mat. Chem. Phys. 141 (2013) 502-511. https://doi.org/10.1016/j.matchemphys.2013.05.050

[36] G. Masi, A. Balbo, J. Esvan, C. Monticelli, J. Avila, L. Robbiola, E. Bernardi, M. C. Bignozzi, M. C. Asensio, C. Martini, C. Chiavari, X-ray Photoelectron Spectroscopy as a tool to investigate silane-based coatings for the protection of outdoor bronze: The role of alloying elements, Appl. Surf. Sci. 433 (2018) 468–479. https://doi.org/10.1016/j.apsusc.2017.10.089

[37] C. Chiavari, E. Bernardi, A. Balbo, C. Monticelli, S. Raffo, M.C. Bignozzi, C. Martini, Atmospheric corrosion of fire-gilded bronze: corrosion and corrosion protection during accelerated ageing tests, Corros. Sci. 100 (2015) 435–447. https://doi.org/10.1016/j.corsci.2015.08.013

[38] F. Cao, Z. Shi, J. Hofstetter, P.J. Uggowitzer, G. Song, M. Liu, A. Atrens, Corrosion of ultra-high-purity Mg in 3.5% NaCl solution saturated with $Mg(OH)_2$, Corros. Sci., 75 (2013) 78-99. https://doi.org/10.1016/j.corsci.2013.05.018

[39] K. Marušić, H. Otmačić Ćurković, Š. Horvat-Kurbegović, H. Takenouti, E. Stupnišek-Lisac, Comparative studies of chemical and electrochemical preparation of artificial bronze patinas and

their protection by corrosion inhibitor, Electrochimica Acta 54 (2009) 7106–7113.

https://doi.org/10.1016/j.electacta.2009.07.014

[40] R. Bostan, S. Varvara, L. Găină, L.M. Muresan, Evaluation of some phenothiazine derivatives

as corrosion inhibitors for bronze in weakly acidic solution, Corros. Sci. 63 (2012) 275–286.

https://doi.org/10.1016/j.corsci.2012.06.010

[41] J.R. Macdonald, Impedance Spectroscopy, Wiley, New York, 1987, p. 1.

[42] J.B. Jorcin, M.E. Orazem, N. Pébère, B. Tribollet, CPE analysis by local electrochemical

impedance spectroscopy, Electrochim. Acta 51 (2006) 1473-1479.

https://doi.org/10.1016/j.electacta.2005.02.128

[43] C.H. Hsu, F. Mansfeld, Concerning the Conversion of the Constant Phase Element Parameter

Y0 into a Capacitance, Corrosion 57 (2001) 747-748. https://doi.org/ 10.5006/1.3280607

[44] G.J. Brug, A.L.G. van den Eeden, M. Sluyters-Rehbach, J.H. Sluyters, The analysis of electrode

impedances complicated by the presence of a constant phase element, J. Electroanal. Chem. 176

(1984) 275. https://doi.org/10.1016/S0022-0728(84)80324-

[45] A. Dermaj, N. Hajjaji, S. Joiret, K. Rahmouni, A. Srhiri, H. Takenouti, V. Vivier, Electrochemical

and spectroscopic evidences of corrosion inhibition of bronze by a triazole derivative, Electrochim.

Acta 52 (2007) 4654–4662. https://doi.org/10.1016/j.electacta.2007.01.068

[46] S. Varvara, L. Muresan, K. Rahmouni, H. Takenouti, Evaluation of some non-toxic thiadiazole

derivatives as bronze corrosion inhibitors in aqueous solution, Corros. Sci. 50 (2008) 2596–2604.

https://doi.org/10.1016/j.corsci.2008.06.046

[47] X T. Wang, J. Wang, Y. Wu, The inhibition effect and mechanism of L -cysteine on the corrosion of bronze covered with a CuCl patina, Corros. Sci. 97 (2015) 89–99. https://doi.org/10.1016/j.corsci.2015.04.018

[48] K. Rahmouni, H. Takenouti, N. Hajjaji, A. Srhiri, L. Robbiola, Protection of ancient and historic bronzes by triazole derivatives, Electrochim. Acta 54 (2009) 5206–5215. https://doi.org/10.1016/j.electacta.2009.02.027

[49] S. Varvara, R. Bostan, O. Bobis, L. Găină, F. Popa, V. Mena, R.M. Souto, Propolis as a green corrosion inhibitor for bronze in weakly acidic solution, Appl. Surf. Sci. 426 (2017) 1100–1112. https://doi.org/10.1016/j.apsusc.2017.07.230

[50] W. Qafsaoui, A. Et Taouil, M.W. Kendig, H. Cachet, S. Joiret, H. Perrot, H. Takenouti, Coupling of electrochemical, electrogravimetric and surface analysis techniques to study dithiocarbamate/bronze interactions in chloride media, Corros. Sci. 130 (2018) 190–202. https://doi.org/10.1016/j.corsci.2017.10.034

[51] A. Mezzi, E. Angelini, T. De Caro, S. Grassini, F. Faraldi, C. Riccucci, G. M. Ingo, Investigation of the benzotriazole inhibition mechanism of bronze disease, Surf. Interface Anal. 44 (2012) 968 – 971. https://doi.org/10.1002/sia.4841

[52] F. Sinapi, S. Julien, D. Auguste, L. Hevesi, J. Delhalle, Z. Mekhalif, Monolayers and mixed-layers on copper towards corrosion protection, Electrochim. Acta 53 (2008) 4228–4238. https://doi.org/10.1016/j.electacta.2007.12.061

[53] L. Kövér, Z. Kovács, R. Sanjinés, G. Moretti, I. Cserny, G. Margaritondo, J. Pálinkás H. Adachi, Electronic structure of tin oxides: high-resolution study of XPS and Auger spectra, Surf. Interfa. 23 (1995) 461–466. https://doi.org/10.1002/sia.740230705

[54] L. Robbiola, T.T.M. Tran, P. Dubot, O. Majerus, K. Rahmouni, Characterisation of anodic layers on Cu-10Sn bronze (RDE) in aerated NaCl solution, Corros. Sci. 50 (2008) 2205–2215. https://doi.org/10.1016/j.corsci.2008.06.003

[55] P. Sinsermsuksakul, L. Sun , S.W. Lee , H.H. Park , S.B. Kim , C. Yang, R.G. Gordon, Overcoming efficiency limitations of SnS-based solar cells, Adv. Energy Mater. Adv. Energy Mater. 2014, 1400496. https://doi.org/10.1002/aenm.201400496

[56] J.A. Rodriguez, T. Jirsak, S. Chaturvedi, J. Hrbek, Surface chemistry of SO_2 on Sn and Sn/Pt(111) alloys: effects of metal-metal bonding on reactivity toward sulfur, J. Am. Chem. Soc. 120 (1998) 11149–11157. https://doi.org/10.1021/ja982174a

[57] M. Hutchison, P. Zhou, K. Ogle, J. Scully, Enhanced electrochemical Cu release from commercial Cu-Sn alloys: fate of the alloying elements in artificial perspiration, Electrochim. Acta (2017). https://doi.org/10.1016/j.electacta.2017.04.092

[58] M. Chan, A. Capek, D.A. Brill, S.J. Garrett, Characterization of the patina formed on a low tin bronze exposed to aqueous hydrogen sulfide, Surf. Interface Anal. 46 (2014) 433-441. https://doi.org/10.1002/sia.5520

[59] G. Masi, C. Chiavari, J. Avila, J. Esvan, S. Raffo, M.C. Bignozzi, M.C. Asensio, L. Robbiola, C. Martini, Corrosion investigation of fire-gilded bronze involving high surface resolution spectroscopic imaging, Appl. Surf. Sci., 366 (2016) 317-327. https://doi.org/10.1016/j.apsusc.2016.01.101

[60] M. Finšgar, EQCM and XPS analysis of 1,2,4-triazole and 3-amino-1,2,4-triazole as copper corrosion inhibitors in chloride solution, Corros. Sci. 77 (2013) 350–359. https://doi.org/10.1016/j.corsci.2013.08.026

[61] L. Yang, J. Huang, L. Cao, L. Shi, Q. Yu, X. Kong, Y. Jie, pH-regulated template-free assembly of Sb$_4$O$_5$Cl$_2$ hollow microsphere crystallites with self-narrowed bandgap and optimized photocatalytic performance, Scientific Reports, 6:27765, DOI: 10.1038/srep27765.

https://doi.org/10.1038/srep27765

[62] E. Paparazzo, L. Moretto, Surface and interface microchemistry of archaeological objects studied with X-ray Photoemission Spectroscopy and scanning Auger microscopy, J. Electron. Spectrosc. Relat. Phenom. 76 (1995) 653-658. https://doi.org/10.1016/0368-2048(95)02429-8

[63] M. Finšgar, 2-mercaptobenzimidazole as a copper corrosion inhibitor: part II. Surface analysis using X-ray photoelectron spectroscopy, Corros. Sci. 72 (2013) 90–98.

https://doi.org/10.1016/j.corsci.2013.03.010

[64] S. Li, S. Shi, G. Huang, Y. Xiong, S. Liu, Synergetic tuning charge dynamics and potentials of Ag$_3$PO$_4$ photocatalysts with boosting activity and stability by facile in-situ fluorination, Appl. Surf. Sci. 455 (2018) 1137–1149. https://doi.org/10.1016/j.apsusc.2018.06.027

[65] V. Di Castro, F. Allegretti, C. Baldacchini, M.G. Betti, G. Contini, V. Corradini, F. Lamastra, C. Mariani, Growth of 2-mercaptobenzoxazole on Cu(100) surface: chemisorbed and physisorbed phases, Surf. Sci. 507–510 (2002) 7–11. https://doi.org/10.1016/S0039-6028(02)01166-4

[66] B.V. Appa Rao, M.N. Reddy, Formation, characterization and corrosion protection efficiency of self-assembled 1-octadecyl-1H-imidazole films on copper for corrosion protection, Arabian Journal of Chemistry (2017) 10, S3270–S3283. https://doi.org/10.1016/j.arabjc.2013.12.026

Figure captions

Figure 1 Structural formulas of the Schiff bases studied as bronze corrosion inhibitors.

Figure 2 Polarization curves recorded on bronze after 1 h of immersion in ARX10 solution: a) in the absence (1) and in the presence of SITP (2), MSITP (3) and TPIE (4); b) in the absence (1) and in the presence of PMSI (5) and SIAP (6).

Figure 3 Polarization curves recorded on bronze after 480 h of immersion in ARX10 solution: a) in the absence (1) and in the presence of SITP (2), MSITP (3), TPIE (4) and PMSI (5); b) comparison of experimental and calculated E/j curves to evaluate the corrosion current density, jcor.

Figure 4 Polarization curves recorded on bronze after 480 h of immersion in ARX10 solution in the absence (1) and in the presence of SITP (2), SITP+ P (3) and only P (4)**.**

Figure 5 Nyquist diagrams from EIS tests carried out on bronze exposed to ARX10 solution for (a) 1 to 48 h and for (b) 168 to 480 h. The complete spectra obtained after 1h and 480 h are shown in the insets.

Figure 6 Equivalent circuits (EC) with three (a) or two (b, c) time constants, used to fit the experimental EIS spectra.

Figure 7 Time evolution of the calculated resistance (a-d) and capacitance (e-g) values, during immersion of bronze in ARX10 solution in the absence and in the presence of SITP and SITP + P.

Figure 8 Nyquist diagrams from EIS tests carried out on bronze immersed for different times in ARX10 solution in the presence of SITP (a) and SITP + P (b). The insets show the complete spectra obtained after 1h in the presence of SITP (a) and SITP + P (b).
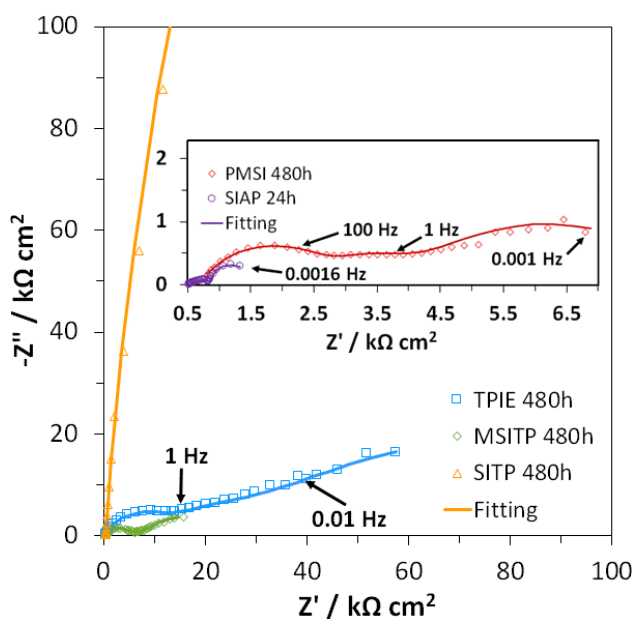
Figure 9 Nyquist diagrams from EIS tests carried out on bronze immersed for 480 h to ARX10 solution in the presence of the different Schiff bases. In the case of SIAP (inset), the spectrum was recorded after 24 h of immersion.

Figure 10 Time evolution of R_p (a) and E_{cor} (b) values during immersion of bronze specimens in ARX10 solution, in the absence and in the presence of the Schiff bases.

Figure 11 BSE-SEM micrographs obtained on bare bronze samples (a) and on samples after 1h (b,d,f) or 480 h (c,e,g) of immersion in ARX10 solution, both in the absence of inhibitors and in the presence of SITP or SITP + P.

Figure 12 XPS surveys spectra on the reference unexposed bronze sample (a) and on bronze specimens exposed for 480 h (b) to ARX10 solution non containing (black), or containing SITP and SITP+P.

Figure 13 XPS core level spectra of C1s (a), N1s (b), O1s (c), S2p (d), Cu Auger LMM (e), Cu2p (f), Sn3d (g) and Pb4f (h), collected on the unexposed sample and on samples exposed for 480 h to uninhibited (Blank) or inhibited (SITP o SITP+P) ARX10 solution.

Table 1 Corrosion potentials (E_{cor}), corrosion current densities (j_{cor}), anodic and cathodic Tafel slopes (b_a, b_c) and inhibiting efficiencies calculated from both j_{cor} (that is η) and from polarization resistance values (η_{Rp}), after 480 h of immersion in ARX10 solution, in the absence and in the presence of the Schiff bases. All data are presented with their corresponding standard deviations.

	E_{cor} /	j_{cor} /	b_a /	$\lvert b_c \rvert$ /	η /	η_{Rp} /
	V_{SCE}	µA cm^{-2}	mV decade^{-1}	mV decade^{-1}	%	%
Blank	0.055 ± 0.013	8.3 ± 1.1	90.2 ± 6.7	∞	--	--
SITP	0.017 ± 0.015	0.0082 ± 0.0025	170 ± 16	200 ± 13	99.91 ± 0.03	99.91 ± 0.04
MSITP	0.054 ± 0.013	1.92 ± 0.62	92.3 ± 5.4	530 ± 41	77.3 ± 6.8	83.3 ± 5.1
TPIE	0.036 ± 0.024	0.46 ± 0.21	76.1 ± 8.2	420 ± 58	94.6 ± 2.3	96.1 ± 2.5
PMSI	0.072 ± 0.020	5.1 ± 1.0	64.1 ± 5.8	∞	33 ± 11	36 ± 21
SITP +P	0.078 ± 0.018	0.018 ± 0.010	290 ± 11	270 ± 14	99.83 ± 0.09	99.91 ± 0.04
P	0.024 ± 0.012	6.0 ± 1.8	60.2 ± 7.1	180 ± 15	19 ± 18	11 ± 15

Table 2 XPS elemental analysis (global composition normalized to 100%) obtained from high-resolution core level spectra of unexposed bronze samples and samples exposed for 480 h to ARX10 solution both in the absence of inhibitors and in the presence of SITP or SITP + P.

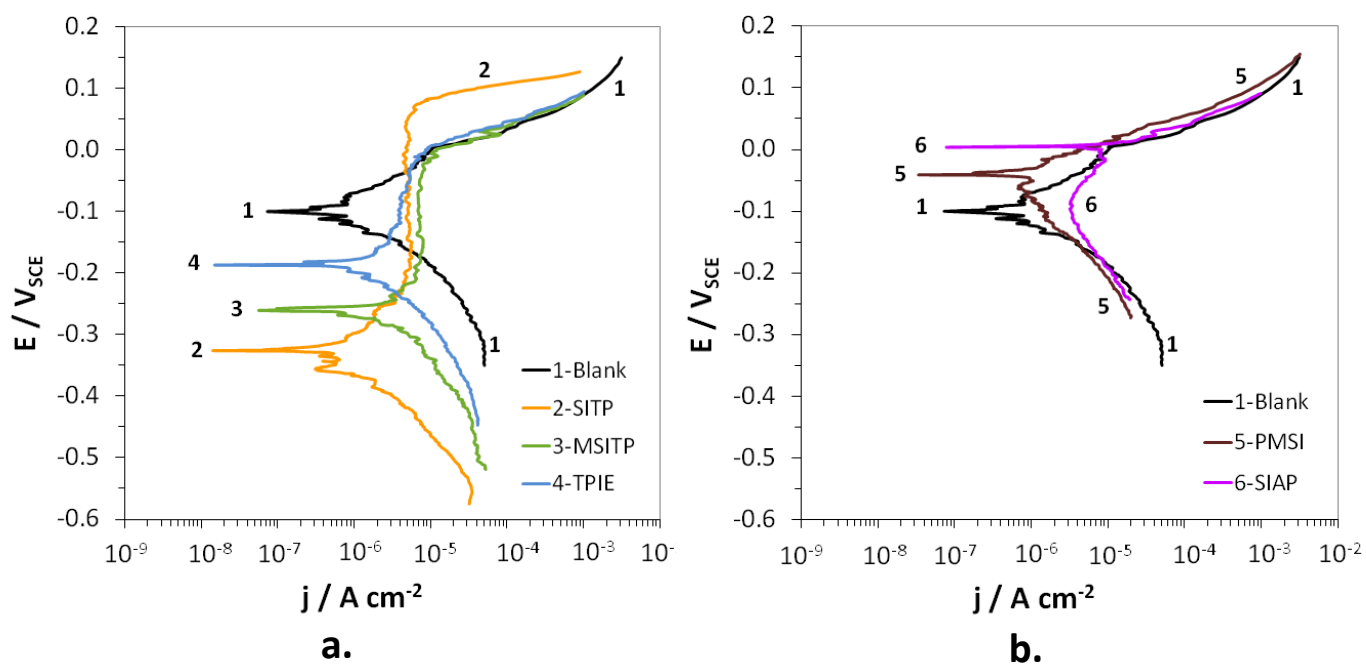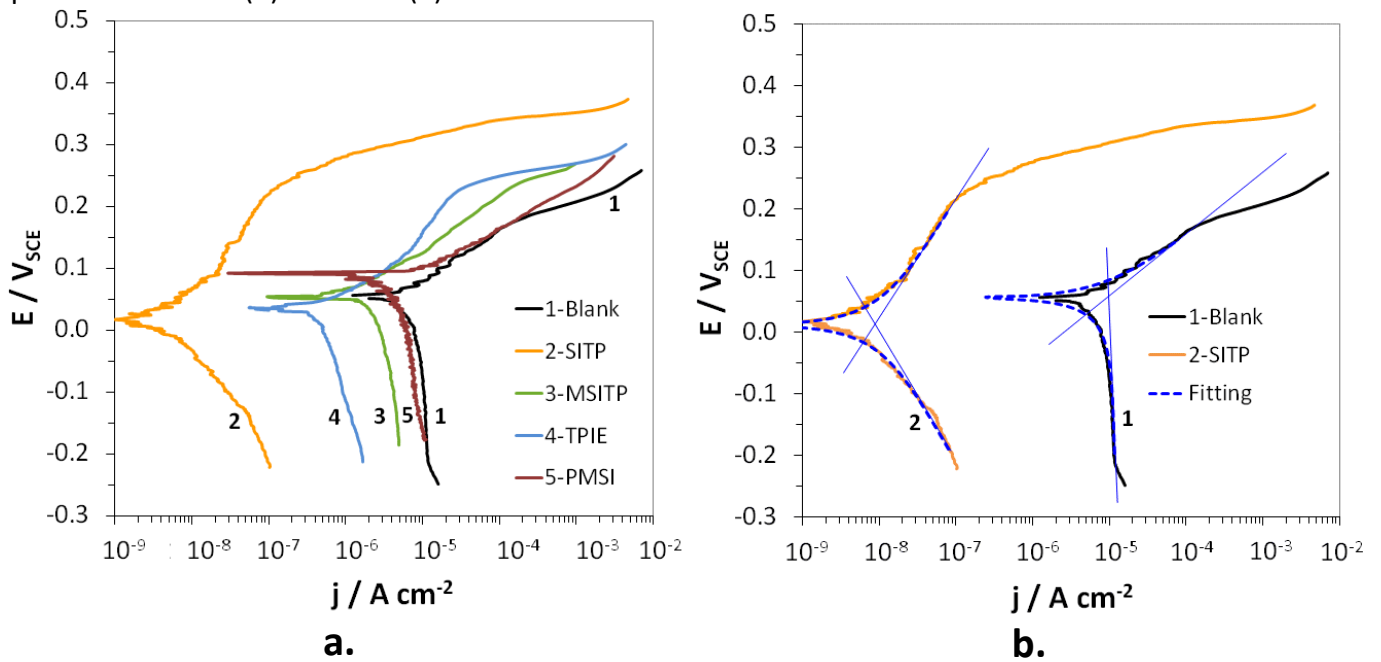| Specimen	C 1s			N 1s	O 1s #	P 2p	S 2p$_{3/2}$			Cu 2p$_{3/2}$		Sn 3d$_{5/2}$			Sb 3d$_{3/2}$	Pb 4f$_{7/2}$
	CC, CH	C-O*, C-S, C-N	C=O, O-C=O	NC, NH			S-Metal	SH, S-C, …	Sulfate …	(Cu°) Cu(I)	Cu(II)	Sn°	Sn(II) (SnO)	Sn (IV) (SnO$_2$)	oxide (s)	PbO-like (s)
Not exposed																
BE (eV)	284.4	286.0	287.3 & 288.2		531.3	-	-	-	-	932.5	934.0	484.7	485.8	-	-	138.1
at. %	42.5	5.2*	7.5		31.1					7.2	1.6	<0.1	0.3	-	-	4.7
Blank 480h																
BE (eV)	284.5	286.0	287.6 & 288.7	399.6	531.0	-	-	-	-	932.3	934.5	-	-	486.7	540.1	138.5
at. %	17.1	11.7	8.2	1.8	40.2					4.8	4.6			8.1	2.2	1.3
SITP 480h																
BE (eV)	284.4	285.8	287.5	399.2	532.0		162.3	163.5	167.4	932.7	934.5	-	-	-	-	-
at. %	48.6	14.2	4.7	7.9	11.6		3.5	5.5	0.9	2.5	0.7					
SITP + P 480h																
BE (eV)	284.5	286.1	288.0	399.5	531.5	132.9	162.3	163.7	167.7	932.6	934.6	-	-	-	-	-

at. %	48.0	15.3	3.2	6.5	16.0	0.2	2.2	3.7	1.8	1.2	2.0

very broad peak including oxide, hydroxide, C-O and sulfate bindings

SITP,
2-(Salicylideneimino) thiophenol

SIAP,
 2-(Salicylideneimino) aminophenol

MSITP,
2-(3-Methoxy-Salicylideneimino) thiophenol

PMSI,
N,N'-O-phenylen-Bis(3-Methoxy-Salicylideneimine)

TPIE,
[2-(2-Thiophenyl)imino]-1,2-diphenylethanone

Figure 1 Structural formulas of the Schiff bases studied as bronze corrosion inhibitors.

a.

b.

Figure 2 Polarization curves recorded on bronze after 1 h of immersion in ARX10 solution: a) in the absence (1) and in the presence of SITP (2), MSITP (3) and TPIE (4); b) in the absence (1) and in the presence of PMSI (5) and SIAP (6).

a.

b.

Figure 3 Polarization curves recorded on bronze after 480 h of immersion in ARX10 solution: a) in the absence (1) and in the presence of SITP (2), MSITP (3), TPIE (4) and PMSI (5); b) comparison of experimental and calculated E/j curves to evaluate the corrosion current density, jcor.

Figure 4 Polarization curves recorded on bronze after 480 h of immersion in ARX10 solution in the absence (1) and in the presence of SITP (2), SITP+ P (3) and only P (4).

Figure 5 Nyquist diagrams from EIS tests carried out on bronze exposed to ARX10 solution for (a) 1 to 48 h and for (b) 168 to 480 h. The complete spectra obtained after 1h and 480 h are shown in the insets.


Figure 6 Equivalent circuits (EC) with three (a) or two (b, c) time constants, used to fit the experimental EIS spectra.
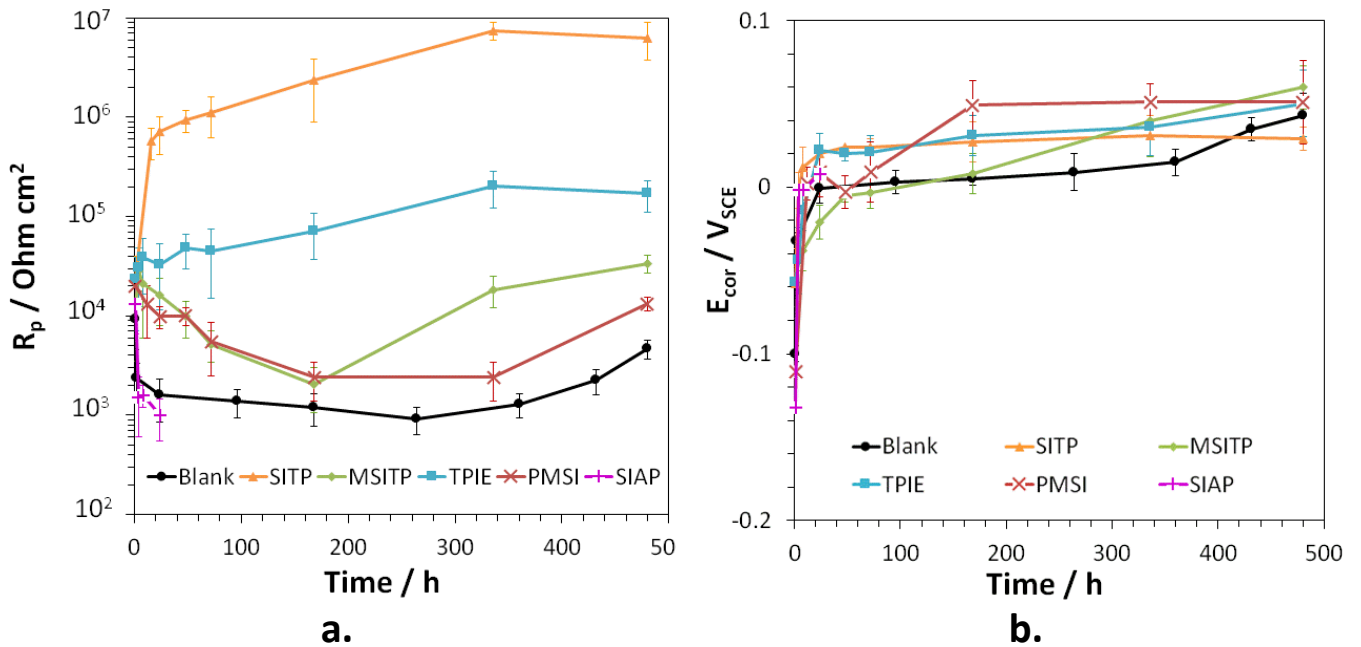
a.

b.

c.

d.

e.

f.

g.

Figure 7 Time evolution of the calculated resistance (a-d) and capacitance (e-g) values, during immersion of bronze in ARX10 solution in the absence and in the presence of SITP and SITP + P.
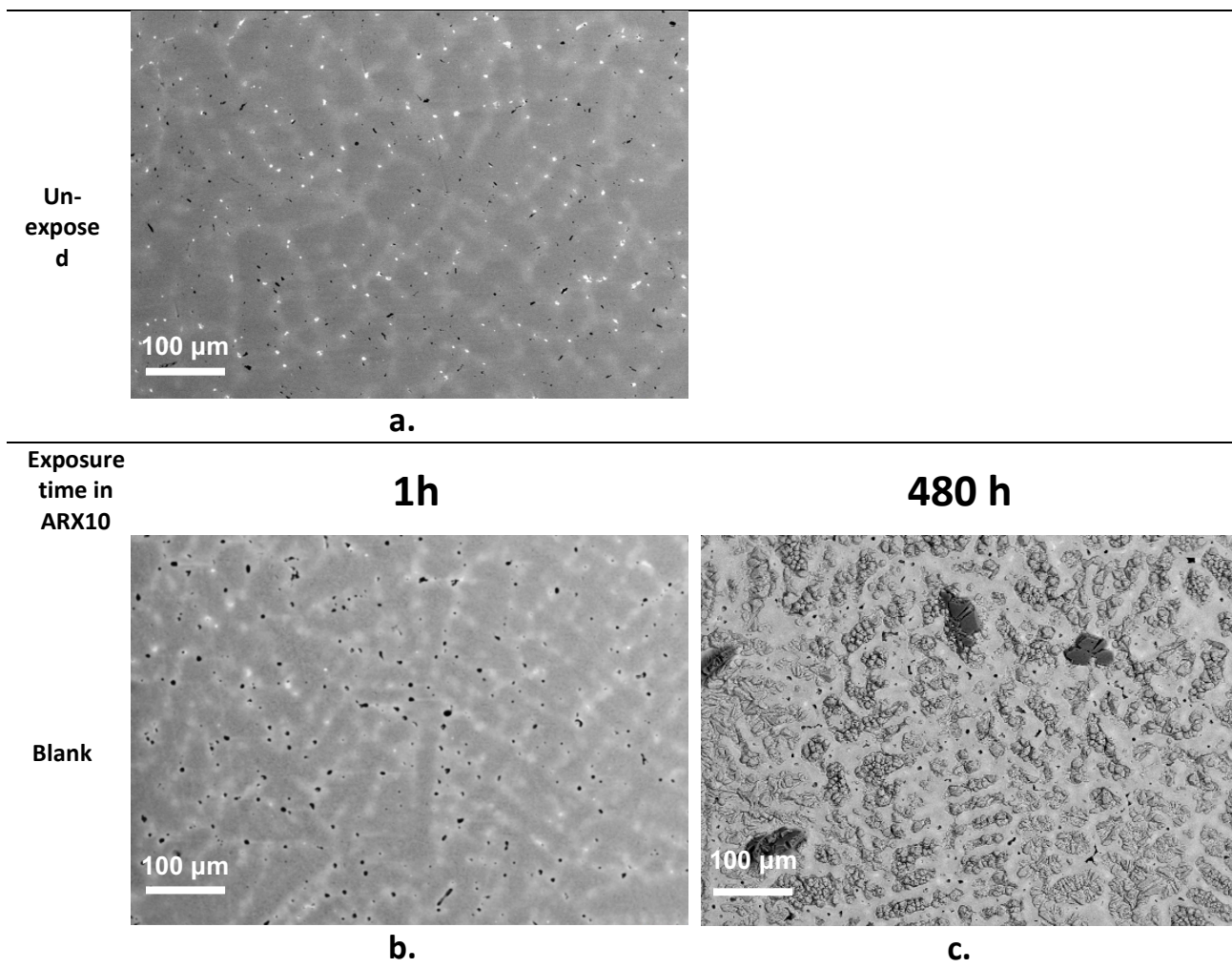

a.

b.

Figure 8 Nyquist diagrams from EIS tests carried out on bronze immersed for different times in ARX10 solution in the presence of SITP (a) and SITP + P (b). The insets show the complete spectra obtained after 1h in the presence of SITP (a) and SITP + P (b).

Figure 9 Nyquist diagrams from EIS tests carried out on bronze immersed for 480 h to ARX10 solution in the presence of the different Schiff bases. In the case of SIAP (inset), the spectrum was recorded after 24 h of immersion.
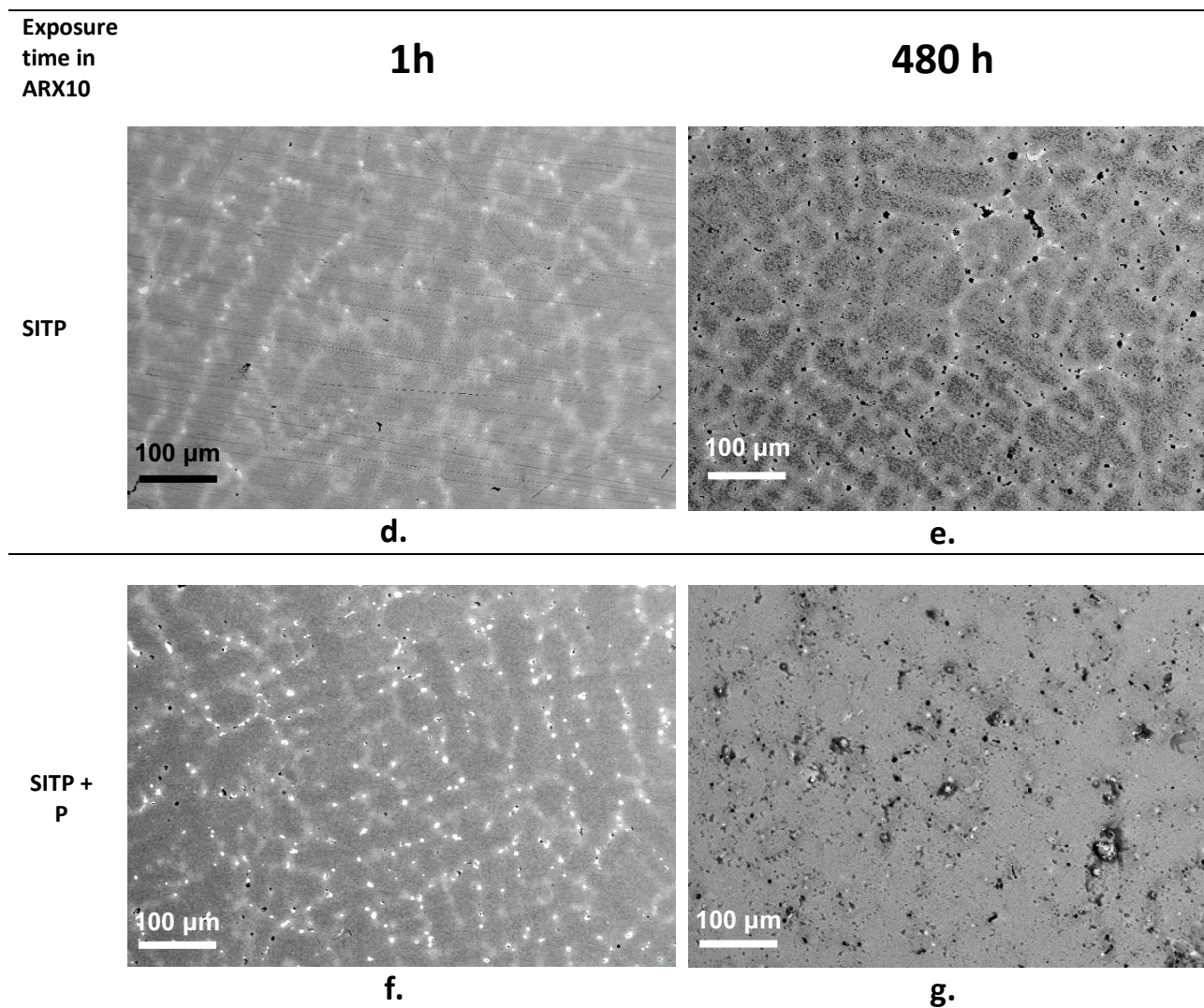

a.

b.

Figure 10 Time evolution of R_p (a) and E_{cor} (b) values during immersion of bronze specimens in ARX10 solution, in the absence and in the presence of the Schiff bases.

Un-exposed

100 μm

a.

Exposure time in ARX10
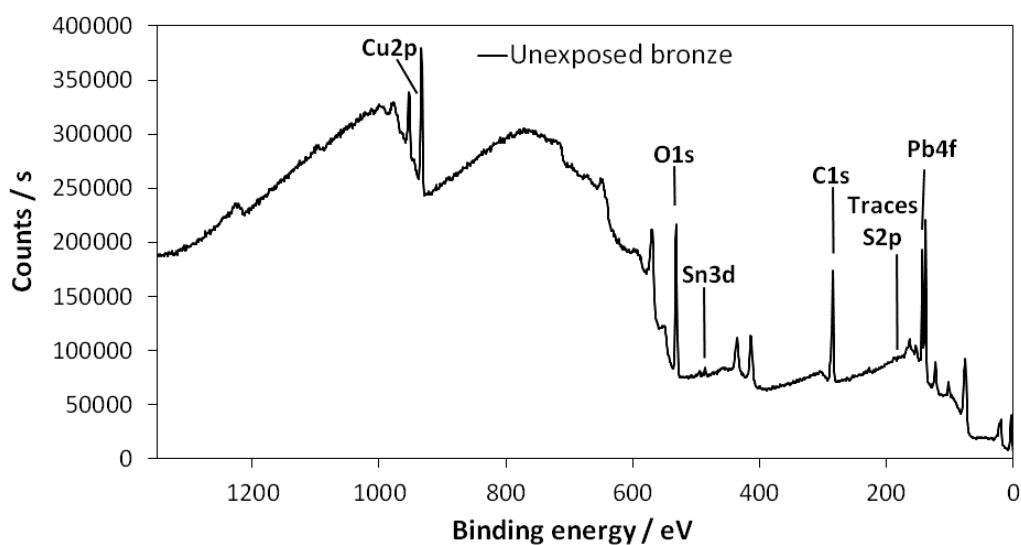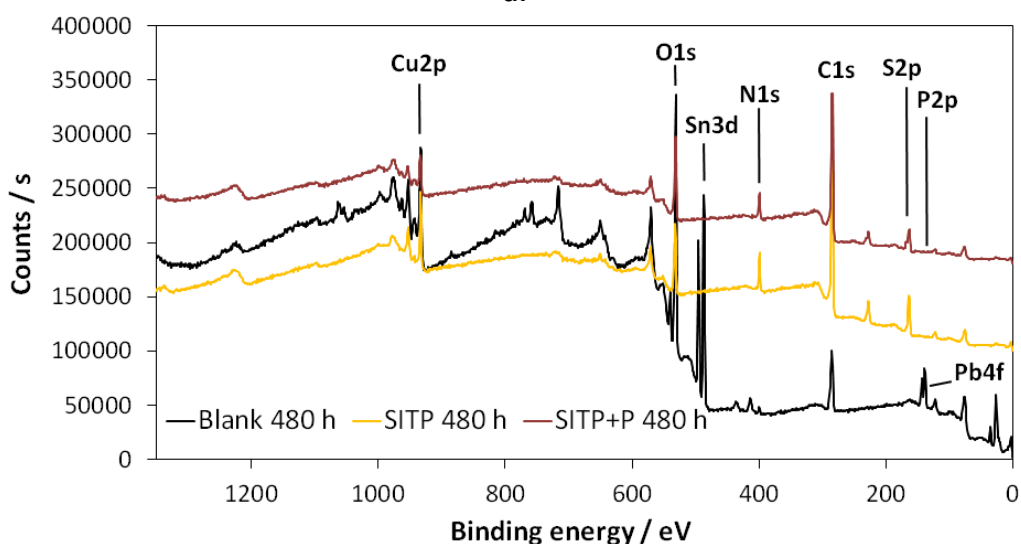
1h

480 h

Blank

100 μm

100 μm

b.

c.

Figure 11 BSE-SEM micrographs obtained on bare bronze samples (a) and on samples after 1h (b,d,f) or 480 h (c,e,g) of immersion in ARX10 solution, both in the absence of inhibitors and in the presence of SITP or SITP + P.

Exposure time in ARX10	**1h**	**480 h**
SITP	100 µm **d.**	100 µm **e.**
SITP + P	100 µm **f.**	100 µm **g.**

Figure 11 BSE-SEM micrographs obtained on bare bronze samples (a) and on samples after 1h (b,d,f) or 480 h (c,e,g) of immersion in ARX10 solution, both in the absence of inhibitors and in the presence of SITP or SITP + P.
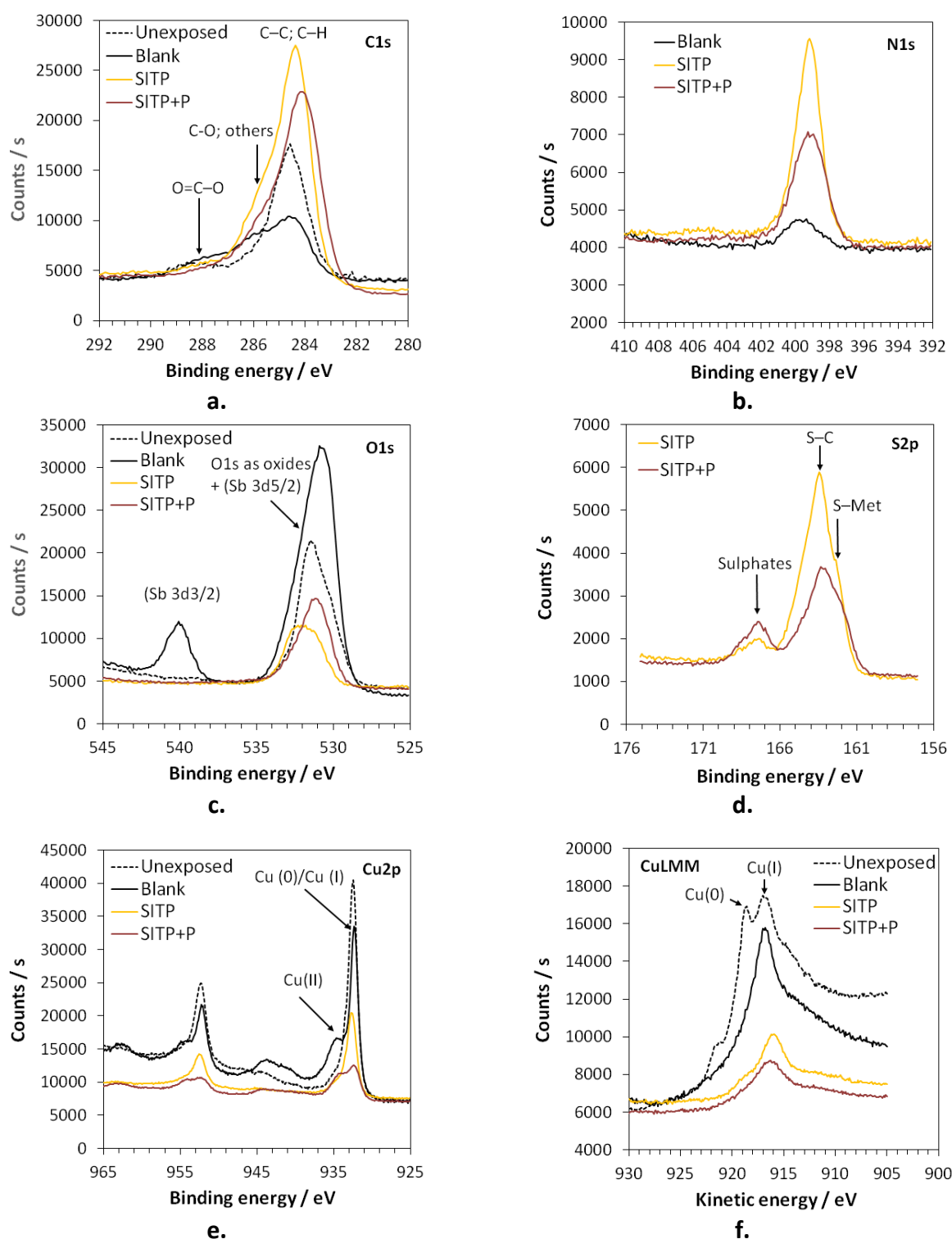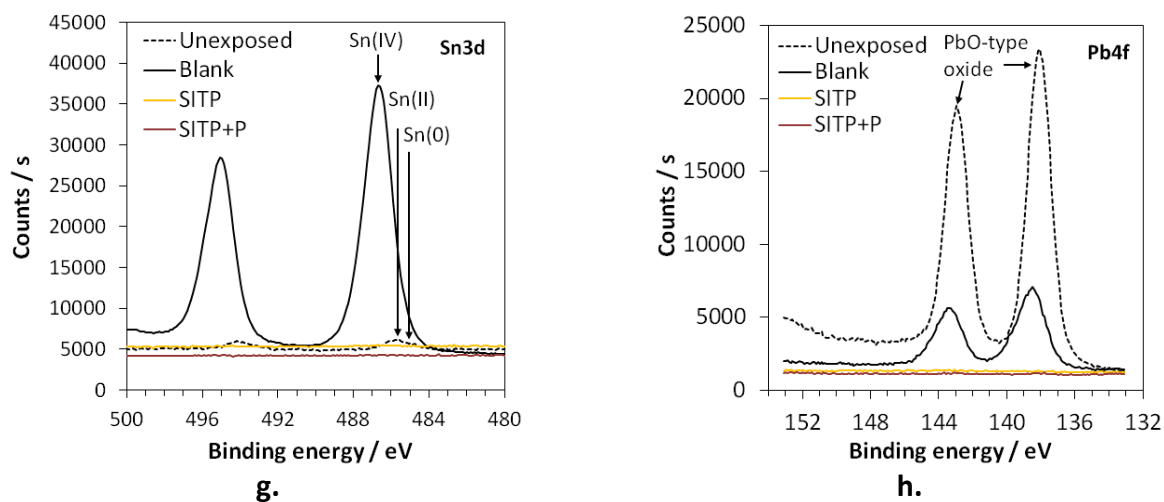
Figure 12 XPS surveys spectra on the reference unexposed bronze sample (a) and on bronze specimens exposed for 480 h (b) to ARX10 solution non containing (black), or containing SITP and SITP+P.

Figure 13 XPS core level spectra of C1s (a), N1s (b), O1s (c), S2p (d), Cu Auger LMM (e), Cu2p (f), Sn3d (g) and Pb4f (h), collected on the unexposed sample and on samples exposed for 480 h to uninhibited (Blank) or inhibited (SITP o SITP+P) ARX10 solution.

Figure 13 XPS core level spectra of C1s (a), N1s (b), O1s (c), S2p (d), Cu Auger LMM (e), Cu2p (f), Sn3d (g) and Pb4f (h), collected on the unexposed sample and on samples exposed for 480 h to uninhibited (Blank) or inhibited (SITP o SITP+P) ARX10 solution.